Eur. Phys. J. E **12**, 111–117 (2003)
DOI 10.1140/epje/i2003-10045-3

THE EUROPEAN PHYSICAL JOURNAL E

Direct visualisation of homogeneous and heterogeneous crystallisation in an ensemble of confined domains of poly(ethylene oxide)

M.V. Massa, J.L. Carvalho, and K. Dalnoki-Veress[a]

Department of Physics & Astronomy and the Brockhouse Institute for Materials Research, McMaster University, Hamilton, ON, L8S 4M1 Canada

Received 1 January 2003 /
Published online: 30 October 2003 –

Abstract. We present a study of homogeneous and heterogeneous nucleation in polymer crystallisation. In bulk samples the crystallization is typically dominated by nucleation from defects (heterogeneous nucleation), and consequently studies must rely on sample preparation to minimize this effect. We present a study of nucleation within discrete droplets of poly(ethylene oxide) that are formed by the dewetting of a thin film on an unfavourable substrate. The samples provide an ensemble of impurity-free droplets, with length scales that can easily be measured. We show that the data for heterogeneous and homogeneous nucleation is qualitatively different, and that the data mirrors the fundamental differences in the underlying mechanisms for the two nucleation processes. The experiments presented here provide a simple method that can be used to study heterogeneous and homogeneous nucleation in great detail.

PACS. 61.41.+e Polymers, elastomers, and plastics – 68.55.-a Thin film structure and morphology – 81.10.-h Methods of crystal growth; physics of crystal growth

1 Introduction

Semi-crystalline polymers are commonplace, yet aspects of crystallisation in polymers, are still poorly understood and enthusiastically debated [1–5]. In order to gain understanding there has been much recent activity focused on systems in confinement [6–29]. One reason for exploring confinement effects is that confined systems are becoming increasingly widespread as devices and materials are constrained due to miniaturisation. In addition, fundamental insight can be gained as the confinement length scale approaches intrinsic length scales of the system studied. The latter may prove useful in gaining a better understanding for crystallisation in the bulk.

There have been several approaches used to study confined systems. A very fruitful avenue has been confinement of crystalline domains in the many micro-phases of block copolymer systems. For example, confinement in one-, two- and three-dimensions can be realised in the lamellar, cylindrical, and spherical micro-phases [6–11,22,23]. The block copolymer systems are somewhat limited by the fact that each new length-scale requires the synthesis of a new polymeric system. This limitation is overcome by confinement in thin films (one-dimensional confinement), since the preparation of various thicknesses can be trivial [12–21,24–29].

The *crystallisation rate* (the rate with which a material crystallises) depends on both the *crystal nucleation rate* and the *crystal growth rate* [1]. While most of the work on polymers has focused on the crystallisation rate [7–14], or the growth rate of individual crystals [15–21], relatively little work has been carried out on the nucleation rate of crystals [22,23,30–34]. The difficulty associated with studying nucleation rate is that there are two mechanisms by which nucleation can occur: *heterogeneous* and *homogeneous* nucleation. Heterogeneous nucleation occurs due to defects in the system (substrate defects, chain defects, contaminants, addition of nucleating agents, etc.) which can pre-dispose a site to nucleate at the defect. The effect of such a heterogeneity is to reduce the energy barrier to nucleation. The second mechanism by which crystals can nucleate, homogeneous nucleation, is spontaneous in origin (self-nucleating). Work by Olmsted, Ryan and coworkers focused on the formation of heterogeneous nucleation sites and observed spinodal density fluctuations as a precursor to this process [35,36]. By comparison to the defects which facilitate nucleation at heterogeneous sites, the homogeneous mechanism has a higher activation barrier, and as a result requires the greatest supercooling. In practice this means that for most systems heterogeneities

[a] e-mail: dalnoki@mcmaster.ca

cause the nucleation of crystals, making homogeneous nucleation elusive. One very elegant approach to study nucleation was first used by Vonnegut to study tin [37] and later adapted by others to study various metallic and organic systems [38,30–34]. The approach is conceptually very simple: if a system is subdivided into a greater number of isolated compartments than the number of heterogeneities, then some of the compartments *must* be void of defects. The compartments free of defects can only nucleate via a homogeneous process. The typical approach to creating small volumes is to disperse droplets (through phase separation, or by using an atomiser) in some other medium [37,38,30–34]. The time scale of crystal growth is typically very short compared to the time scale of nucleation because the droplets are small. This separation of time scales makes studying nucleation, independently from crystal growth, possible. More recent approaches have used the micro-phases in block copolymer systems to prepare small volumes of crystallisable material in order to study crystallisation kinetics [7–11,22,23].

An important study by Reiter and co-workers recently introduced a different approach to studying nucleation: atomic-force microscopy (AFM) was used to *directly visualise* crystallisation of poly(ethylene oxide) (PEO) in the spherical domains of a diblock copolymer [23]. Reiter *et al.* found that the system needed large supercooling in order to facilitate homogeneous nucleation. The crystallisation could be resolved in time and space. It was found that there was no correlation between neighbouring spherical sites.

In this paper we focus on the kinetics of homogeneous and heterogeneous nucleation. Optical microscopy is used to investigate nucleation in small domains in a manner that is very similar to some of the early work using droplets dispersed in a low molecular-weight medium [38, 30–34]. The samples used in this study are dewetted films of PEO on a polystyrene (PS) substrate. Though there are still some outstanding questions, the general process of dewetting is by now fairly well understood [39–41]. In particular, from dewetting studies we know that it is possible to control a broad distribution of droplet sizes by changing the film thickness of the dewetting layer. For small droplets where gravity can be ignored, in equilibrium each "droplet" is a spherical cap (there can be a small deviation from this near the contact line). The geometry of the spherical caps is defined by the contact angle of the dewetting material on the substrate. A fundamental difference between work previously carried out and the nucleation study presented here is that the interface of the droplets of PEO is very well defined. In particular, the spherical surface of the droplet is exposed to the ambient atmosphere (Argon or vacuum in this work), while the flat surface of the droplet, the base, is a PS-PEO interface. The PEO film is prepared on a PS substrate which is kept below the glass transition temperature of the PS at all times. As a result, the interfacial width between the droplet and the substrate is expected to be very sharp: ~ 1 nm, based on the interfacial width of an other immiscible system held below the glass transition [42]. In addition, the PS substrate is clean and reproducible, making this an ideal system for the study of nucleation. A further advantage of using dewetted droplets for the study of crystallisation is that the broad distribution of droplet sizes provides an opportunity for the study of the dependence of the nucleation rate on length scale [43].

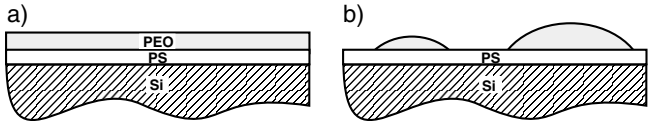

Fig. 1. Schematic diagram of the sample geometry before (a) and after (b) annealing at $T = 90\,^{\circ}$C. After a long annealing treatment the PEO film dewetted into many small droplets on a PS substrate.

2 Experiment

The samples consisted of a clean Si substrate with a bilayer of PEO on top of PS (PEO-PS-Si). All polymer was obtained from Polymer Source (Dorval Quebec, Canada). The PS ($M_{\rm w} = 2\,100\,000$, $M_{\rm w}/M_{\rm n} = 1.16$) was dissolved in toluene (mass fraction of 2%) and spincoated onto the Si substrates at 4000 r.p.m., resulting in a film with thickness $h \sim 200$ nm. These films were then annealed in vacuum at 115 °C for 12 hours to remove any residual solvent, and to relax the polymer chains, as much as possible, into their equilibrium conformation. PEO ($M_{\rm w} = 27\,000$, $M_{\rm w}/M_{\rm n} = 1.09$) was dissolved in acetonitrile (mass fraction of 2.5%) and spincoated onto the PS-Si substrate at 4000 r.p.m., resulting in a PEO film with $h \sim 70$ nm.

After the preparation of the PEO-PS-Si films (Fig. 1a), the samples were annealed in vacuum for long periods of time (> 24 h) at a temperature of $T = 90\,^{\circ}$C. The annealing temperature is well above the observed melting temperature of PEO ($T_{\rm m} \sim 64\,^{\circ}$C) but below the glass transition temperature of the PS substrate ($T_{\rm g} = 98\,^{\circ}$C). Under these conditions, the PEO film dewets on the unfavourable PS substrate resulting in small droplets of PEO (Fig. 1b). After the annealing procedure the sample is transferred (while being held above $T_{\rm m}$) to a commercial microscopy hotstage which is held at 90 °C (Linkam THMS-600, temperature control to within 0.1 °C). The hotstage was flushed at all times with Argon to ensure that the samples were always in a dry atmosphere.

The crystallisation of the PEO droplets was monitored using optical microscopy with nearly crossed polarisers (under the nearly crossed polariser condition, amorphous droplets still show some contrast with the substrate). Image sequences were taken with a CCD camera to follow the crystallisation of the droplets. The amorphous droplets appear dark when viewed with nearly crossed polarisers, and become bright once crystallised. The images enable us to determine the time at which a specific droplet crystallises, as well as the PEO-PS interfacial area of the droplet. In addition, the surface morphology of the crystallized droplets was characterised using atomic-force microscopy (TM microscopes Explorer, Veeco).

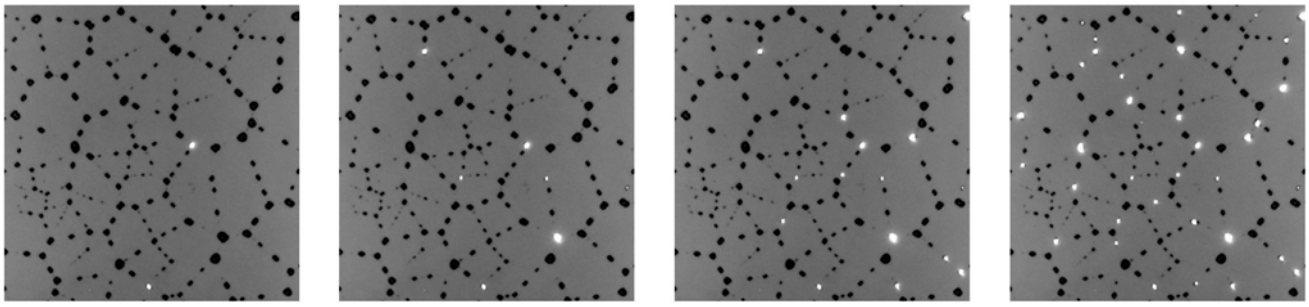

Fig. 2. Series of optical microscopy images of one area of the film. The images were obtained during cooling a sample at 0.4 °C/min starting at $T_c = -2\,°C$ for the first image. The temperature interval between consecutive images is 0.6 °C. Each image is 1000 μm wide. When an amorphous droplet nucleates and becomes semi-crystalline, the droplet appears white under nearly crossed polarisers.

3 Results and discussion

In order to study the homogeneous and heterogeneous nucleation rate in an ensemble of PEO droplets, it is crucial that the droplets are isolated from each other. If this is not the case, then a nucleus in one droplet will cause the crystallisation of a neighbouring droplet. This was especially important since previous observations by Reiter and coworkers has shown the existence of a single lamellar layer of adsorbed PEO chains in some systems [25–27]. Such an adsorbed layer could be seen around some of our droplets, although the layer never resulted in droplets that were interconnected. By limiting the extent of annealing, it was possible to prepare a sample that had not fully dewetted. In such a case, droplets were often interconnected resulting in a chain of droplets. Once one of the droplets in the chain nucleated, the crystallisation passed from one droplet to its neighbour, until all the droplets in the chain had crystallised. By using long annealing times and verification with AFM, it was possible to ensure that this was not the case for the samples discussed here.

The AFM measurements were also used to obtain the contact angle between the PEO droplet and the PS substrate. We found that, on average, the contact angle was $\theta = (20 \pm 1)°$. In addition the shape of the droplets was, to a good approximation, that of a spherical cap. With such a well-defined geometry it is possible to use the area of the droplet's PEO-PS interface (*i.e.* looking normal to the film surface) to obtain a good estimate of a droplet volume. In order to calculate the volume of the droplets we use the PEO-PS interfacial area (obtained with optical microscopy), the measured contact angle θ, and assume a spherical cap. It is important to realise that even if a droplet is slightly ellipsoidal in shape the error associated with the assumptions made is very small. For the samples discussed here we probe an ensemble of droplets with a broad-size distribution. In this paper we quote the droplet sizes in terms of the surface area of the PEO-PS interface, which corresponds to the "base area" of the droplet. It is the base area that is directly measured with optical microscopy.

The measurements probing the nucleation rate were carried out using optical microscopy in reflection with polarisers. A typical sequence of optical images is shown in Figure 2. It is apparent that from one frame to the next, more droplets become crystalline. From such a sequence it is straightforward to obtain the time at which a droplet crystallises and the base area of each droplet. With our current setup it is possible to simultaneously view ~ 1000 droplets, while still having enough pixels (1300×1030) of the digital image devoted to each droplet so that a meaningful base area could be measured.

In Figure 3 we plot the ratio of the number of crystallised droplets, N_c, to the total number of droplets in the field of view of the microscope, N_∞, as a function of the temperature, T, for droplets ranging in base area from 200 μm^2 to 500 μm^2. The data was obtained by annealing the sample for at least 1/2 hour at 90 °C in argon —a protocol that was used for all samples. The sample was then cooled at a rate of 0.4 °C/min. It is immediately obvious, that there are two distinct regions in the plot of N_c/N_∞ shown in Figure 3a: as the sample is cooled there is a sharp increase in the extent of crystallinity at $T \sim 55\,°C$ and then a plateau is reached with an other sharp increase in the extent of crystallinity at $T \sim -5\,°C$. As will be discussed later, we identify these as a heterogeneous nucleation region and a homogeneous nucleation region, respectively.

Since heterogeneous nucleation is associated with defects in the sample (chain defects, substrate defects, contaminants, etc.) a second sample was prepared which was spincoated from a solution that was passed through a 0.2 μm pore size filter immediately prior to use. The results of this are shown in Figure 3b and are surprising: the peak in crystallisation activity which we ascribe to heterogeneous nucleation has completely disappeared. All the nucleation events occur at a temperature of $T \sim -5\,°C$. This is in agreement (to within $\pm 0.1\,°C$) with the "partially dirty" sample shown in Figure 3a. It should be noted that the preparation of the "partially dirty" sample required many trials. In most cases samples were either "clean" and showed most nucleation at $T \sim -5\,°C$ or "dirty" with almost all nucleation occurring at much higher temperatures.

The comparison of the "partially dirty" and "clean" samples provides convincing proof that the nucleation observed at $T \sim 55\,°C$ is heterogeneous in origin. More

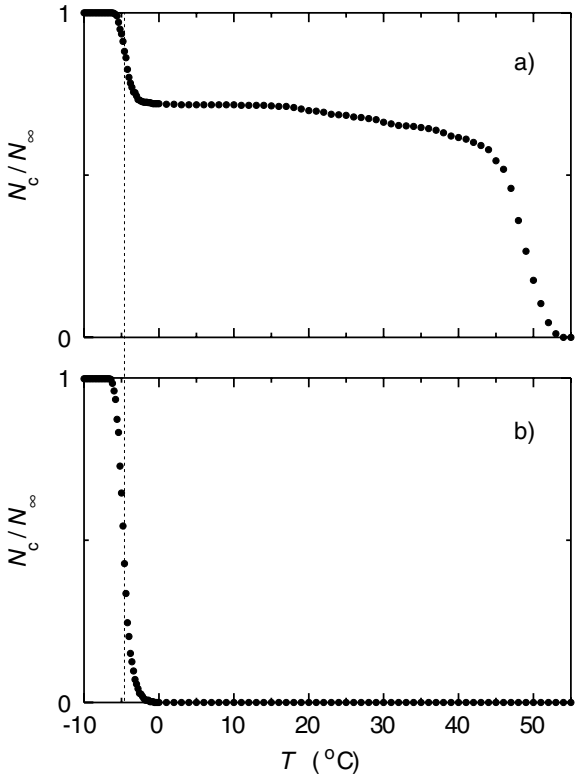

Fig. 3. Plot of the fraction of crystallised droplets (N_c/N_∞) as a function of temperature for a sample that has: a) a high content of heterogeneous nucleation sites, and b) a low content of heterogeneous sites. The samples are annealed above T_m and then cooled at a rate of 0.4 °C/min.

striking evidence of this is obtained if we repeat the cooling experiment on the "partially dirty" sample and compare the same area in the two runs. At a temperature of $T \sim 7\,^\circ$C, there are ~ 1000 droplets of which ~ 700 are crystalline (see Fig. 3a). Comparison of the droplets that have crystallised or remain in the melt in the two runs reveals that less than 1% of the of the droplets differ.

It must be stressed that the preparation of "clean" samples is not only the result of filtering the solution prior to use. Bulk systems typically have many heterogeneous nucleation sites and filtering will not remove them all. The dewetted system is unique. First of all, the dewetting process for films of the thickness described here is due mostly to dust particles and defects —even for the filtered solution. In the first stages of dewetting a hole is formed and AFM or optical microscopy reveals that this hole often has a small dust particle in the middle of it. As a hole grows further, it eventually impinges on other holes and finally forms small droplets [39–41]. This process cleans the droplets further as more contaminants are given the opportunity to migrate to the surface of the droplet, pin at a contact line, and deposit on the PS substrate as the PEO droplets recede. In effect the dewetting process cleans the material, leaving behind small contaminants. The second big difference in the droplet approach compared to bulk samples is that each droplet acts as its own small experiment in an ensemble of thousands of droplets [37,38,30–34]. This is an advantage shared by studies with block copolymer systems where the crystallisable component is confined into spherical micro-domains. In a bulk system, once a nucleation site has been established, the growth of a crystal occurs rapidly until the crystallite runs out of amorphous material —either because it impinges on other crystallites or due to limitations in sample size. For the large supercooling required to see nucleation in the small droplets the growth rate is very rapid compared to the nucleation rate.

The "clean" samples (Fig. 3b) are very reproducibly produced by filtering and dewetting and only a very small fraction ($< 1\%$) of the droplets are crystallised by the heterogeneous process. This can be seen easily in the comparison of the temperature ramps carried out on both types of samples (Fig. 3a and b). Cooling of the sample to $T \sim -5\,^\circ$C resulted in rapid nucleation which we ascribe to a homogeneous process which will be discussed in more detail below. We re-iterate that the small droplets had to be supercooled by $\sim 70\,^\circ$C in order to see the homogeneous process. Such a large supercooling was only possible because 1) the sample volume of each droplet is small resulting in a very low probability of a homogeneous nucleation site occurring in a single droplet, and 2) the droplets are free of defects due to care taken in the sample preparation and especially because the dewetting process is "self-cleaning".

Thus far we have direct evidence, provided by the data shown in Figure 3, that the nucleation that occurs at $T \sim 55\,^\circ$C is heterogeneous in origin. The nucleation which occurred in the droplets at $T \sim -5\,^\circ$C was referred to as homogeneous. While it is appealing to describe the two stages of nucleation shown in Figure 3a as heterogeneous nucleation at higher temperature and homogeneous nucleation at lower temperature, we must rule out the possibility that the lower-temperature activity is simply due to less efficient heterogeneities. In the following we illustrate that the data obtained for nucleation in the two temperature regimes is fundamentally different and is consistent with the different mechanisms associated with heterogeneous and homogeneous nucleation.

As described above, the measurements were performed by annealing the sample at $T = 90\,^\circ$C in argon for 1 hour prior to ramping down the sample temperature. The "partially clean" sample was used to obtain data on the heterogeneous process. Data corresponding to the nucleation rate for droplets ranging in base area from $100\,\mu\text{m}^2$ to $300\,\mu\text{m}^2$ are plotted in Figure 4a, where we show N_c/N_∞ as a function of temperature. The sample is cooled at $0.1\,^\circ$C/min. The data represents a slower cooling experiment when compared to the data shown in Figure 3, and covers a smaller temperature range. From such data it is possible to extract details of the nucleation rate, but because we have a broad distribution of droplet sizes, this requires a more careful analysis taking into account the individual droplet volume. Nucleation rate and the dependence on length scale will be the subject of a forthcoming publication [43].

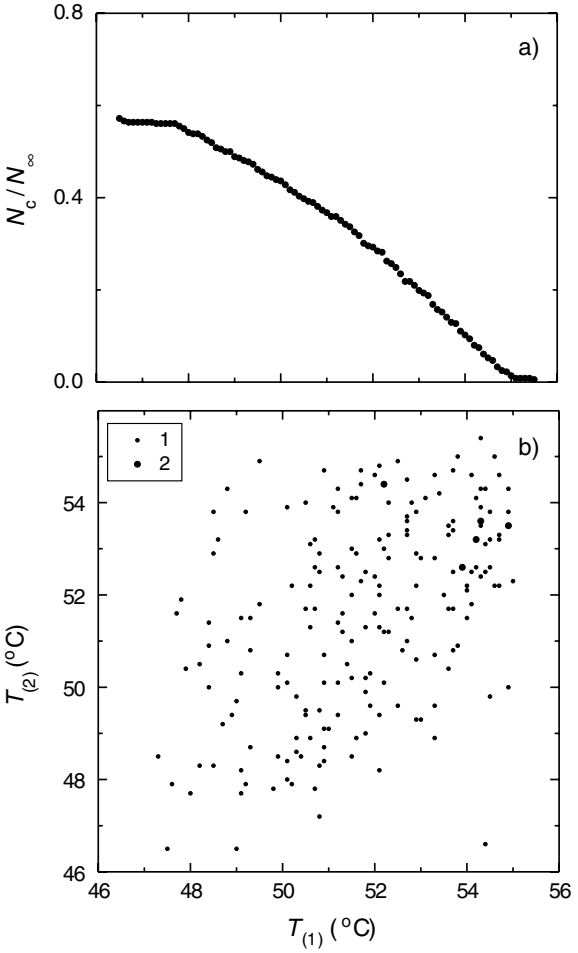

Fig. 4. a) Plot of the fraction of crystallised droplets (N_c/N_∞) as a function of temperature when cooling the sample at 0.1 °C/min. b) A correlation plot of the data for two consecutive runs. The size of the data point indicates the number droplets as indicated in the legend. Heterogeneous droplets will show some correlation from one run to the next, indicating that the data should be clustered around a line with slope 1.

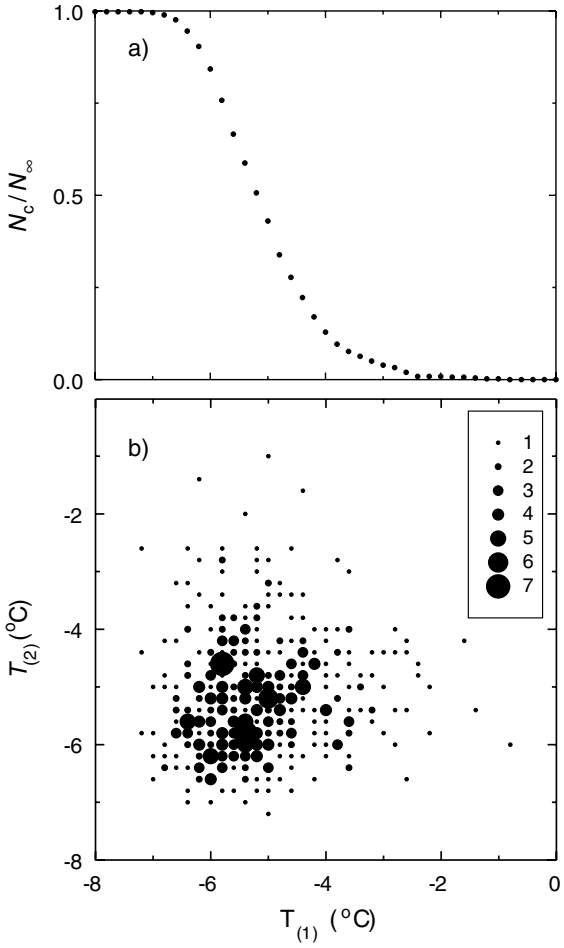

Fig. 5. a) Plot of the fraction of crystallised droplets (N_c/N_∞) as a function of temperature when cooling the sample at 0.4 °C/min. b) A correlation plot of the data for two consecutive runs. The size of the data point indicates the number droplets as indicated in the legend. Homogeneous droplets will not be correlated from one run to the next.

In subsequent crystallisation runs the same field of view is used so that we can keep track of individual droplets and when they crystallise for each run. In Figure 4b we show a correlation plot of the data for two consecutive runs: if droplet "i" crystallised at temperature $T_{(1,i)}$ on the first run and at $T_{(2,i)}$ on the second run, then the droplet is plotted as a point at $(T_{(1,i)}, T_{(2,i)})$. A careful examination of Figure 4b reveals that there is a clear correlation: the data points are roughly localised around a line with slope 1 (*i.e.*, the data is symmetric about the slope 1 line). This is expected: if a droplet is nucleated by a defect, the activation energy will depend on the specific defect. As an example, we compare two droplets with a barrier to nucleation provided by the activation energy ϵ_a and ϵ_b. If $\epsilon_a < \epsilon_b$, then upon cooling there is a greater probability that droplet "a" will nucleate at a higher temperature than droplet "b". When an experiment is repeated on the same droplets, then, *on average*, $T_{(1,a)} \sim T_{(2,a)} > T_{(1,b)} \sim T_{(2,b)}$ resulting in data that is clustered about a line with slope 1. The heterogeneous data shown in Figure 4b follows these expectations.

In order to distinguish between heterogeneous and homogeneous data, we performed a similar cooling experiment near $T = -5\,^\circ$C on "clean" samples. A sample, annealed at $T = 90\,^\circ$C in argon for 1 hour is cooled at 0.4 °C/min from 0 to $-8\,^\circ$C. In Figure 5a we plot the fraction of crystallised droplets (N_c/N_∞) as a function of temperature for droplets ranging in base area from 100 μm^2 to 300 μm^2 —the exact same droplet range as that used for the heterogeneous case.

The conclusive evidence for the difference between heterogeneous and homogeneous nucleation is illustrated in Figure 5b. It is clear that the data is symmetric about a point corresponding to a temperature $T = 5.5\,^\circ$C for both consecutive runs. This point of symmetry corresponds to the temperature at which the rate of crystal nucleation is the highest. The data is not elongated along a line with a slope of 1 as in the case of heterogeneous data. Again this result, while new, is to be expected: the energy barrier

to nucleation is a function of the PEO itself and is the same in each droplet. If we assume an equal size for all droplets, then all droplets have an equal probability of having a nucleation event. As a result the data should not show a correlation (*i.e.* not be clustered along a line with slope 1). In fact, the assumption of equal droplet size is not entirely valid since Figure 5 reports on droplets with base areas ranging from $100\,\mu m^2$ to $300\,\mu m^2$. A careful look at the data in Figure 5b reveals that there is a *very slight* elongation of the data along the line with slope 1 as a result of different droplet size. The elongation is because larger droplets are more likely to have a nucleation event than a smaller droplet. A detailed analysis of the dependence of homogeneous nucleation on length scale will be reported in a forthcoming publication [43].

4 Conclusions

The data shown in this paper are the result of a unique sample geometry which results in small droplets. Each individual droplet in this ensemble of droplets acts as a mini-experiment. We are able to show *in a single sample* both heterogeneous and homogeneous nucleation. Cooling crystallisation runs reveal two distinct temperatures at which nucleation activity is high, with a heterogeneous nucleation process occurring for a higher temperature than the homogeneous nucleation process. Most exciting are the correlation plots which conclusively show that the data for heterogeneous and homogeneous nucleation are qualitatively different. This reflects the differences in the underlying mechanisms for the two nucleation processes. It is typically very difficult, if not impossible, to do experiments on homogeneously nucleated crystallisation because the data is overwhelmed by the much higher nucleation rate of the heterogeneous process. Practically, this means that a typical sample is fully crystallised before statistically significant homogeneous nucleation can be observed. The broad distribution of droplet sizes obtained in dewetted samples will enable future studies of the dependence of the nucleation rate on the length scale [43]. The methodology and analysis presented here provides a tool with which both heterogeneous and homogeneous nucleation can be unambiguously identified and characterised in great detail.

We thank Prof. James Forrest for useful discussions. Financial support from NSERC of Canada, the Canadian Foundation for Innovation and the Ontario Innovation Trust is gratefully acknowledged.

References

1. G. Strobl, *The Physics of Polymers: Concepts for Understanding their Structures and Behaviour*, second edition (Springer-Verlag, Berlin, 1997).
2. G. Strobl, Eur. Phys. J. E **3**, 165 (2000).
3. B. Lotz, Eur. Phys. J. E **3**, 185 (2000).
4. S.Z.D. Cheng, C.Y. Li, L. Zhu, Eur. Phys. J. E **3**, 195 (2000).
5. M. Muthukumar, Eur. Phys. J. E **3**, 198 (2000).
6. S. Hong, W.J. MacKnight, T.P. Russell, S.P. Gido, Macromolecules **34**, 2883 (2001).
7. B. Lotz, A.J. Kovacs, Kolloid Z. Z. Polym. **209**, 97 (1966).
8. B. Lotz, A.J. Kovacs, ACS Polym. Prepr. **10**, 820 (1969).
9. L. Zhu, B.H. Calhoun, Q. Ge, R.P. Quirk, S.Z.D. Cheng, E.L. Thomas, B.S. Hsiao, F. Yeh, L. Liu, B. Lotz, Macromolecules **34**, 1244 (2001).
10. P.A. Weimann, D.A. Hajduk, C. Chu, K.A. Chaffin, J.C. Brodil, F.S. Bates, J. Polym. Sci. Part B, Polym. Phys. **37**, 2053 (1999).
11. S. Nojima, M. Toei, S. Hara, S. Tanimoto, S. Sasaki, Polymer **43**, 4087 (2002).
12. C.W. Frank, V. Rao, M.M. Despotopoulou, R.F.W. Pease, W.D. Hinsberg, R.D. Miller, J.F. Rabolt, Science **273**, 912 (1996).
13. M.M. Despotopoulou, C.W. Frank, R.D. Miller, J.F. Rabolt, Macromolecules **29**, 5797 (1996).
14. M.M. Despotopoulou, R.D. Miller, J.F. Rabolt, C.W. Frank, J. Polym. Sci. Part B, Polym. Phys. **34**, 2335 (1996).
15. J.V. Mclaren, Polymer **4**, 175 (1963).
16. S. Sawamura, H. Miyaji, K. Izumi, S.J. Sutton, Y. Miyamoto, J. Phys. Soc. Jpn. **67**, 3338 (1998).
17. K. Izumi, G. Ping, M. Hashimoto, A. Toda, H. Miyaji, Y. Miyamoto, Y. Nakagawa, in *Advances in the Understanding of Crystal Growth Mechanisms*, edited by T. Nishinaga, K. Nishioka, J. Harada, A. Sasaki, H. Takei (Elsevier Science, Amsterdam, 1997) p. 337.
18. R. Pearce, G.J. Vancso, Macromolecules **30**, 5843 (1997).
19. Yu. K. Godovsky, S.N. Magonov, Langmuir **16**, 3549 (2000).
20. K. Dalnoki-Veress, J.A. Forrest, M.V. Massa, A. Pratt, A. Williams, J. Polym. Sci. Part B, Polym. Phys. **38**, 2564 (2000).
21. M.V. Massa, K. Dalnoki-Veress, J.A. Forrest, Eur. Phys. J. E **11**, 191 (2003).
22. Y.-L. Loo, R.A. Register, A.J. Ryan, Phys. Rev. Lett. **84**, 4120 (2000).
23. G. Reiter, G. Castelein, J.-U. Sommer, A. Röttele, T. Thurn-Albrecht, Phys. Rev. Lett. **87**, 226101 (2001).
24. K. Taguchi, H. Miyaji, K. Izumi, A. Hoshino, Y. Miyamoto, R. Kokawa, Polymer **42**, 7443 (2001).
25. G. Reiter, J.-U. Sommer, Phys. Rev. Lett. **80**, 3771 (1998).
26. G. Reiter, J.-U. Sommer, J. Chem. Phys. **112**, 4376 (2000).
27. J.-U. Sommer, G. Reiter, J. Chem. Phys. **112**, 4384 (2000).
28. Y. Sakai, M. Imai, K. Kaji, M. Tsuji, J. Cryst. Growth **203**, 244, (1999).
29. J. Kressler, C. Wang, H.W. Kammer, Langmuir **13**, 4407 (1997).
30. R.L. Cormia, F.P. Price, D. Turnbull, J. Chem. Phys. **37**, 1333 (1962).
31. J.A. Koutsky, A.G. Walton, E. Baer, J. Appl. Phys. **38**, 1832 (1967).
32. P.J. Barham, D.A. Jarvis, A. Keller, J. Polym. Sci. Part B, Polym. Phys. **20**, 1733 (1982).
33. M.L. Arnal, A.J. Müller, P. Maiti, M. Hikosaka, Macromol. Chem. Phys. **201**, 2493 (2000).
34. A.J. Müller, M.L. Arnal, F. López-Carrasquero, Macromol. Symp. **183**, 199 (2002).

35. P.D. Olmsted, W.C.K. Poon, T.C.B. McLeish, N.J. Terrill, A.J. Ryan, Phys. Rev. Lett. **81**, 373 (1998).
36. E.L. Heeley, C.K. Poh, W. Li, A. Maidens, W. Bras, I.P. Dolbnya, A.J. Gleeson, N.J. Terrill, J.P. Fairclough, P.D. Olmsted, R.I. Ristic, M.J. Hounslow, A.J. Ryan, Faraday Discuss. **122**, 343 (2002).
37. B. Vonnegut, J. Colloid Sci. **3**, 563 (1948).
38. D. Turnbull, R.L. Cormia, J. Chem. Phys. **34**, 820 (1961).
39. C. Redon, F. Brochard-Wyart, F. Rondelez, Phys. Rev. Lett. **66**, 715 (1991).
40. G. Reiter, Phys. Rev. Lett. **68**, 75 (1992).
41. S. Herminghaus, K. Jacobs, K. Mecke, J. Bischof, M. Ibn-Elhaj, Schlagowski, Science **282**, 916 (1998).
42. J.A. Forrest, K. Dalnoki-Veress, J. Polym. Sci. Part B, Polym. Phys. **39**, 2664 (2001).
43. Michael V. Massa, Kari Dalnoki-Veress, to be published (2003).